https://doi.org/10.5194/egusphere-2025-6389
Preprint. Discussion started: 24 February 2026

A Continuous Implicit Neural Representation Framework with Gradient Regularization for Sea Surface Height Reconstruction From Satellite Altimetry

Dongshuang Li[1,2], Liming Pan[3], Zhaoyuan Yu[4,5], and Linwang Yuan[4,5]

[1]College of Marine Science and Engineering, Nanjing Normal University, Nanjing, China
[2]Jiangsu Key Laboratory of Ocean-Land Environmental Change and Ecological Construction, Nanjing Normal University, Nanjing, China
[3]School of Cyber Science and Technology, University of Science and Technology of China, Hefei, China
[4]Key Laboratory of Virtual Geographic Environment, Ministry of Education, Nanjing Normal University, Nanjing, China
[5]Jiangsu Center for Collaborative Innovation in Geographical Information Resource Development and Application, Nanjing, China

Correspondence: Liming Pan (pan_liming@ustc.edu.cn)

Abstract. Satellite altimetry provides valuable measurements of sea surface height (SSH) but is characterized by irregular spatiotemporal sampling and substantial data gaps arising from orbital configurations, sensor limitations, and environmental conditions. These sampling properties pose challenges for constructing continuous and dynamically consistent SSH fields. In this study, we develop an interpolation framework based on implicit neural representations (INRs), in which SSH is represented as a continuous function of space and time. The framework employs sinusoidal representation networks (SIREN) to enable smooth gradients and efficient spectral representation. To improve reconstruction in regions with sharp spatial transitions, such as fronts and eddy boundaries, we incorporate a total variation (TV) regularization term, allowing the model to preserve abrupt features while maintaining global smoothness. The combination of a continuous, differentiable INR formulation with gradient-based regularization provides a compact and flexible approach for SSH reconstruction. We evaluate the proposed framework using both multi-mission satellite altimetry observations and high-resolution numerical simulations. Experiments conducted indicate that the proposed SIREN–TV framework can recover fine-scale and locally sharp structures while preserving the large-scale variability of the SSH field. The method maintains a level of global accuracy comparable to existing interpolation and data-assimilation approaches, but provides enhanced spatial detail in regions affected by strong gradients, fronts, or mesoscale activity. In addition, the continuous and fully differentiable representation enables direct computation of spatial derivatives, facilitating higher-order oceanographic diagnostics. These results suggest that INR-based formulations offer a promising complementary avenue for SSH interpolation under sparse and irregular sampling configurations.

https://doi.org/10.5194/egusphere-2025-6389
Preprint. Discussion started: 24 February 2026

1 Introduction

Satellite altimetry provides the primary observational foundation for estimating sea surface height (SSH), a key variable for understanding ocean circulation, sea-level variability, and large-scale climate processes. Gridded SSH products derived from satellite altimetry are widely used in oceanographic research, supporting analyses of mesoscale and submesoscale dynamics and their role in the global ocean energy budget (Srinivasan and Tsontos, 2023). However, altimetric observations are inherently limited by sensor capabilities, atmospheric interference (e.g., clouds and precipitation), and orbital configurations, which together lead to irregular spatiotemporal sampling and substantial data gaps (Fablet et al., 2021).These limitations pose significant challenges for reconstructing SSH fields that are continuous and capable of resolving small-scale variability from incomplete observations (Shi and Jin, 2024).

Over the past decades, numerous algorithmic approaches have been developed to address the SSH mapping problem. The Data Unification and Altimeter Combination System (DUACS) represents the most established operational framework, relying on space–time optimal interpolation (OI) to merge multi-mission altimeter observations into gridded products (Le Traon and Dibarboure, 1999). The DUACS system provides robust large-scale SSH estimates and resolves oceanic features down to 150–200 km in wavelength at midlatitudes. Nevertheless, OI's linear statistical formulation limits its ability to capture nonlinear ocean processes, resulting in the loss or smoothing of mesoscale and submesoscale structures such as fronts and eddies (Stegner et al., 2021). Many studies have sought to enhance the space–time resolution of gridded SSH products. The dynamical optimal interpolation (DOI) framework incorporates a dynamical constraint based on potential vorticity conservation into the optimal interpolation procedure (Ubelmann et al., 2015). This approach demonstrated improved representation of fine-scale structures that are typically smoothed or filtered out by conventional DUACS products. More recently, the back-and-forth nudging (BFN-QG) approach introduces a dynamical constraint derived from quasigeostrophic dynamics into the assimilation procedure, enhancing the resolution of SSH reconstructions (Le Guillou et al., 2021). Despite these advances, enhancing the reconstruction resolution of gridded altimetry products remains an ongoing challenge.

In recent years, data-driven and artificial intelligence (AI)-based algorithms have been proposed to address problems directly related to oceanography. Notably, preliminary results indicate promising potential for reconstructing and predicting sea surface conditions from partial and noisy satellite observations (Manucharyan et al., 2021; Lou et al., 2023; Camargo et al., 2023; Denvil-Sommer et al., 2023). The concept behind data-driven interpolation is to utilize machine learning to estimate values based on patterns and statistical relationships derived from training data, rather than relying on external instructions and assumptions. Despite these advances, most existing approaches still rely on discrete grid-based representations, which limit spatial continuity and restrict resolution by predefined sampling intervals.

To overcome the limitations of discrete grid-based formulations, implicit representations have emerged as an alternative framework for modeling continuous fields. Instead of storing discrete values at fixed grid points, an implicit representation models a field as a continuous function that maps coordinates to signal values, allowing fine-scale structures to be captured without being constrained by grid resolution. Recent advances in computer vision and graphics have demonstrated that fully connected neural networks can serve as continuous and memory-efficient implicit representations for geometric entities such

https://doi.org/10.5194/egusphere-2025-6389
Preprint. Discussion started: 24 February 2026

as shape components (Genova et al., 2019), objects (Oechsle et al., 2019), and scenes (Sitzmann et al., 2019). These models, known as Implicit Neural Representations (INRs), parameterize continuous functions using multi-layer perceptrons (MLPs) that learn coordinate-to-value mappings for complex spatial or spatiotemporal signals (Xu et al., 2022).

Beyond their conceptual elegance, INRs possess several properties that make them particularly attractive for scientific field reconstruction. Defined on a continuous domain, INRs are highly memory-efficient and can represent fine-scale variability limited only by the capacity of the network architecture (Huang et al., 2021). Their differentiable formulation allows analytical computation of gradients and higher-order derivatives via automatic differentiation, independent of fixed grids. As a result, INRs have been successfully applied to shape modeling (Ye et al., 2022), texture synthesis (Guan et al., 2023), inverse problems (Molaei et al., 2023), and generative modeling (Wiesner et al., 2022). However, their adoption in the Earth sciences remains limited, particularly in oceanographic contexts. Motivated by these advantages, this study leverages INRs to learn a continuous representation from sparse altimetry observations and to reconstruct high-resolution SSH fields across the domain.

The representational capacity of an INR depends critically on the design of its neural architecture. Conventional MLPs often struggle to represent high-frequency variations, which has motivated several architectural refinements. For instance, coordinate-based networks frequently employ Fourier Feature Mapping to enhance the modeling of fine-scale details, but this approach can lead to noisy or unstable gradients (Tancik et al., 2020). An alternative formulation, the Sinusoidal Representation Network (SIREN), introduces periodic (sine) activation functions within fully connected networks to operate directly in the spectral domain (Sitzmann et al., 2020). This design facilitates the representation of complex, high-frequency structures while maintaining smooth and differentiable signal continuity. In this study, we adopt the SIREN formulation for its simplicity, differentiability, and strong spectral representation capacity.

In satellite altimetry data, SSH generally exhibits smooth spatial variations; however, localized abrupt changes may arise due to influences such as seabed topography, mesoscale eddies, wave activity, or storm events. These discontinuities are of particular importance, as they reflect critical dynamical processes within the ocean system. Therefore, an effective SSH reconstruction method must not only capture the large-scale continuous structure but also accurately represent these regions of sharp variation. The standard SIREN architecture, which optimizes a loss function based solely on the difference between predicted and observed values, performs well in reconstructing smoothly varying patterns. Nonetheless, its ability to represent abrupt or high-gradient features remains limited. This shortcoming reduces its effectiveness for SSH reconstruction tasks, where both smooth and discontinuous spatial behaviors are essential to capture.

To address this limitation, we incorporate total variation (TV) regularization into the SIREN framework. TV regularization penalizes excessive oscillations in the reconstructed field by minimizing the spatial and temporal gradients of the solution, thereby encouraging piecewise smoothness while preserving sharp transitions. This property is particularly advantageous for SSH reconstruction, where the underlying field is generally smooth but may exhibit abrupt variations due to strong oceanic fronts, eddies, or storm-induced disturbances. By constraining spurious oscillations and enhancing edge preservation, the TV-enhanced SIREN effectively balances global smoothness with the ability to resolve local discontinuities. This modification enables more accurate and physically interpretable SSH reconstructions from sparse and irregular satellite observations.

https://doi.org/10.5194/egusphere-2025-6389
Preprint. Discussion started: 24 February 2026

In the proposed framework, satellite altimetry observations are first expressed as irregularly sampled coordinate–value pairs, where each sample consists of spatial–temporal coordinates and the corresponding measured SSH. These coordinates are used as continuous inputs to the SIREN network, which learns a mapping from the coordinate domain to SSH values. The network parameters are optimized by minimizing a composite loss function that combines a data fidelity term and a TV regularization term. The data term constrains the network to fit the observed SSH values, while the TV term enforces spatial–temporal smoothness and suppresses nonphysical oscillations. This joint objective allows the model to reconstruct SSH fields that are both consistent with the available observations and capable of representing sharp gradients where strong oceanic variability occurs. During training, the model progressively refines the underlying continuous SSH function, enabling reconstruction and differentiation at arbitrary resolutions.

The remainder of this paper is organized as follows. Section 2 reviews the relevant background and related work, with an emphasis on INRs and the SIREN framework. Section 3 formulates the SSH reconstruction problem. Section 4 presents the proposed reconstruction framework, including the SIREN-based implicit representation and the regularization strategy designed to preserve sharp spatial features. Section 5 reports the experimental results obtained from both real satellite altimetry observations and simulated SSH fields. Finally, Section 6 concludes the paper and discusses the main findings, along with potential directions for future research.

2 Background and related work

2.1 Implicit Neural Representations

Implicit Neural Representations (INRs) are coordinate-based neural networks that model continuous scalar or vector fields by learning a mapping $\Phi : \mathbb{R}^m \to \mathbb{R}^n$ from spatial–temporal coordinates to corresponding physical quantities. In the context of SSH modeling, $\Phi(x, y, t)$ represents the SSH value at a specific location (x, y) and time t. Unlike discrete, grid-based representations, INRs define the signal on a continuous domain, enabling sub-grid interpolation and compact memory representation.

Formally, an INR can be viewed as a function implicitly defined by a relation $F(\mathbf{x}, \Phi, \nabla_{\mathbf{x}}\Phi, \nabla^2_{\mathbf{x}}\Phi, \dots) = 0$, where Φ and its derivatives satisfy certain physical or observational constraints. In practical applications, the goal is to find a function Φ that satisfies a set of N such constraints $\{\mathcal{C}(\Phi, a_i \mid \Omega_j)\}_{j=1}^{N}$, where $\mathcal{C}$ denotes a differentiable functional relating Φ to observed quantities a_i over domains $\Omega_j \subseteq \mathbb{R}^m$. This can be formulated as an optimization problem:

$$\Phi^* = \arg\min_{\Phi} \sum_{j=1}^{N} \|\mathcal{C}(\Phi, a_i \mid \Omega_j)\|_2 , \tag{1}$$

where Φ is typically parameterized by a fully connected neural network. The parameters are optimized using gradient descent, allowing the model to learn a continuous representation that conforms to the available observations.

INRs have been successfully applied to a variety of fields, including shape modeling, texture synthesis, and physical simulations, due to their ability to represent complex, continuous structures with high fidelity. This property makes them a promising

https://doi.org/10.5194/egusphere-2025-6389
Preprint. Discussion started: 24 February 2026

framework for reconstructing oceanographic fields such as SSH, which require both smooth and detailed spatial representations.

2.2 SIREN Framework

Building upon the concept of INRs, most practical INR models adopt coordinate-based MLPs that map spatial or spatio-temporal coordinates to continuous signal values. Let $\mathbf{x} \in \mathbb{R}^m$ denote an input coordinate. A standard INR can be expressed as a composition of affine transformations and nonlinear activations $\Phi(\mathbf{x}) = \mathbf{W}_n \, \phi_{n-1}\big(\cdots \phi_1(\mathbf{x})\big)$, where $\phi_i(\mathbf{z}) = \sigma_i(\mathbf{W}_i \mathbf{z} + \mathbf{b}_i), \quad i = 1, \ldots, n-1$. Traditional INR architectures commonly use ReLU activations. While effective for representing low-frequency variations, ReLU-based networks struggle with high-frequency components and cannot reliably model derivatives because the activation is piecewise linear with zero second derivative almost everywhere (Sitzmann et al., 2020). Smooth activations such as $\tanh$ or $\mathrm{softplus}$ alleviate this limitation to some extent, but often lead to poorly conditioned gradients, making the learning of fine-scale structures difficult.

To address these issues, Sitzmann et al. (2020) proposed the *Sinusoidal Representation Network* (SIREN), which replaces the activation function with a periodic sine:

$$\phi_i(\mathbf{z}) = \sin(\mathbf{W}_i \mathbf{z} + \mathbf{b}_i), \quad i = 1, \ldots, n-1. \tag{2}$$

The sinusoidal activation endows SIREN with several advantageous properties. Since the derivative of $\sin(\cdot)$ is $\cos(\cdot)$, which corresponds to a phase-shifted sinusoid, the network remains closed under differentiation. In other words, any derivative of Φ can be expressed by a network composed of the same sinusoidal units. Consequently, spatial or temporal derivatives $\nabla^k \Phi$ can be computed analytically through automatic differentiation without compromising numerical stability. This property makes SIREN particularly suitable for representing smooth physical fields that demand accurate, high-resolution reconstruction together with reliable gradient information, such as SSH and its spatial variations.

3 Problem Formulation

Satellite radar altimeters provide SSH measurements only along their ground tracks, resulting in sparse and irregular spatio-temporal observations. Let $\mathbf{x}_i = (x_i, y_i, t_i) \in \mathbb{R}^3$ denote the longitude, latitude, and time of the i-th measurement, and let $f(\mathbf{x}_i) \in \mathbb{R}$ be the corresponding SSH value. The dataset can be written as

$$\mathcal{D} = \{(\mathbf{x}_i, f(\mathbf{x}_i))\}_{i=1}^{N}, \tag{3}$$

where each observation provides the SSH at a single spatio-temporal coordinate.

The goal of this work is to reconstruct a continuous SSH field over a prescribed spatio-temporal domain $\Omega \subset \mathbb{R}^3$ from these sparse observations. Formally, we seek a continuous mapping $\Phi : \Omega \to \mathbb{R}$ such that $\Phi(\mathbf{x})$ approximates the true SSH at any location $\mathbf{x} = (x, y, t) \in \Omega$. This formulation naturally aligns with reconstruction problems, where the task is to recover the underlying SSH at unobserved locations based on a limited set of point measurements. Given $\mathcal{D}$, the reconstruction task is cast

https://doi.org/10.5194/egusphere-2025-6389
Preprint. Discussion started: 24 February 2026

as a supervised regression problem. The model parameters θ are obtained by minimizing the empirical discrepancy between predicted and observed SSH values:

$$\mathcal{L}_{\text{data}}(\theta) = \frac{1}{N}\sum_{i=1}^{N}\left[\Phi_\theta(\mathbf{x}_i) - f(\mathbf{x}_i)\right]^2, \tag{4}$$

where $\Phi_\theta(\mathbf{x}_i)$ denotes the model prediction at the coordinate $\mathbf{x}_i$.

Once trained, the function Φ_θ provides a continuous representation of the SSH field, allowing evaluation at arbitrary spatio-temporal coordinates within Ω—including points at which no measurements are available. This implicit formulation enables high-resolution reconstruction of spatially and temporally complete SSH fields from sparse altimetry observations.

4 Proposed Framework

This section presents the proposed INR framework for reconstructing a continuous SSH field from sparse satellite altimetry observations. The approach integrates a SIREN to model fine-scale spatial and temporal variability while total variation (TV) regularization constrains the reconstruction to maintain physical sharpness. Detailed architectural design, normalization strategies, regularization formulation, and training configurations are described below.

4.1 SIREN-based Implicit Neural Representation

Reconstruction of a continuous SSH field is achieved by parameterizing the mapping $\Phi_\theta : (x, y, t) \rightarrow \text{SSH}$ using a SIREN architecture. Since the general properties of SIREN have been reviewed in the Background section, this subsection focuses on the architectural design and implementation choices specific to this work.

4.1.1 Network Architecture

We employ a fully connected network consisting of an input layer, n hidden layers, and a final linear projection. Each hidden layer applies a sinusoidal transformation,

$$\mathbf{z}_{k+1} = \sin(\mathbf{W}_k\mathbf{z}_k + \mathbf{b}_k), \tag{5}$$

and the SSH estimate is produced by $\Phi_\theta(\mathbf{x}) = \mathbf{W}_n\mathbf{z}_n$.

The architecture is configured to balance expressive power and training stability for oceanographic fields that contain both slowly varying background patterns and localized mesoscale fluctuations.

4.1.2 Coordinate Normalization

SSH observations span heterogeneous spatial and temporal scales: longitude and latitude typically cover a range of hundreds of degrees, whereas the temporal domain may extend from days to years depending on the satellite mission. Using raw coordinates leads to ill-conditioned gradients and inconsistent sensitivity across dimensions. To address this issue, each coordinate is

https://doi.org/10.5194/egusphere-2025-6389
Preprint. Discussion started: 24 February 2026

normalized by a dimension-specific scaling factor:

$$\tilde{x} = \mathrm{factor}_s\, x, \qquad \tilde{y} = \mathrm{factor}_s\, y, \qquad \tilde{t} = \mathrm{factor}_t\, t. \tag{6}$$

The spatial factor factor_s maps the geographical domain to an approximately unit-scale range, ensuring uniform response of sinusoidal activations across the spatial extent. The temporal factor factor_t aligns the temporal dynamics with the spatial frequencies learned by the network, which is particularly important given the diverse sampling patterns of multi-mission altimetry (e.g., TOPEX/Poseidon, Jason series, Sentinel-3, HY-2). This normalization substantially improves numerical conditioning, accelerates convergence, and enhances the physical coherence of the reconstructed SSH field.

4.2 Regularization for Sharp-Feature Preservation

While the SIREN-based INR can accurately approximate smooth large-scale SSH patterns, altimetry-derived SSH fields also contain sharp spatial gradients associated with important oceanographic processes. These gradients carry meaningful dynamical information. Elevated values of $\nabla_{\mathrm{lon}}\Phi_\theta$ and $\nabla_{\mathrm{lat}}\Phi_\theta$ typically arise in dynamically active regions of the ocean, including areas influenced by strong western boundary currents, frontal transitions between water masses, mesoscale eddy peripheries and vorticity filaments, as well as coastal zones shaped by bathymetric steering. Preserving these spatial variations is therefore essential for ensuring that the reconstructed SSH field remains physically consistent and dynamically interpretable.

A reconstruction driven solely by data-fitting may oversmooth such sharp features, especially in regions with sparse or irregular observations. To mitigate this issue, we enhance the INR with a total variation (TV) regularization term that selectively penalizes small-scale noise while retaining physically meaningful gradient structures.

Data-Fidelity Loss. Given altimetric observations $\{(\mathbf{x}_i, \mathrm{SSH}_i)\}_{i=1}^N$ with $\mathbf{x}_i = (\mathrm{lon}_i, \mathrm{lat}_i, \mathrm{time}_i)$, the network prediction is $\mathrm{SSH}_{\mathrm{pred},i} = \Phi_\theta(\mathbf{x}_i)$. The data-fitting loss adopts the mean squared error:

$$\mathcal{L}_{\mathrm{data}} = \frac{1}{N}\sum_{i=1}^{N}\left(\mathrm{SSH}_{\mathrm{pred},i} - \mathrm{SSH}_{\mathrm{true},i}\right)^2. \tag{7}$$

Spatial Gradients via SIREN. Let $y(\mathbf{x}) = \Phi_\theta(\mathbf{x})$ denote the reconstructed SSH field. Since SIREN employs sinusoidal activations, y is differentiable with respect to its input coordinates, allowing spatial gradients to be computed analytically:

$$\nabla_{\mathrm{sp}} y(\mathbf{x}) = \left(\frac{\partial y}{\partial \mathrm{lon}}, \frac{\partial y}{\partial \mathrm{lat}}\right) = \left(v_{\mathrm{lon}}, v_{\mathrm{lat}}\right).$$

Total Variation Regularization. To preserve localized sharp transitions while suppressing noise-induced fluctuations, we adopt the first-order isotropic TV penalty:

$$\mathcal{L}_{\mathrm{TV}} = \frac{1}{M}\sum_{j=1}^{M}\sqrt{v_{\mathrm{lon},j}^2 + v_{\mathrm{lat},j}^2}, \tag{8}$$

evaluated over M uniformly sampled spatial points in the reconstruction domain. The TV term encourages sparsity in gradient magnitude, retaining fronts, eddy boundaries, and other dynamically relevant high-gradient features without over-smoothing.

https://doi.org/10.5194/egusphere-2025-6389
Preprint. Discussion started: 24 February 2026

Combined Objective. The final loss balances fidelity to observations and preservation of physically meaningful gradients:

$$\mathcal{L}_{\text{total}} = \mathcal{L}_{\text{data}} + a\mathcal{L}_{\text{TV}}, \tag{9}$$

where $a > 0$ controls the trade-off between smoothness and sharp-feature retention. With an appropriately chosen λ, the reconstructed SSH field captures both the basin-scale background variability and the sharp mesoscale or submesoscale gradients characteristic of real ocean dynamics.

The complete processing pipeline—including coordinate normalization, SIREN-based implicit representation, and TV-regularized optimization—is summarized in Figure 1.

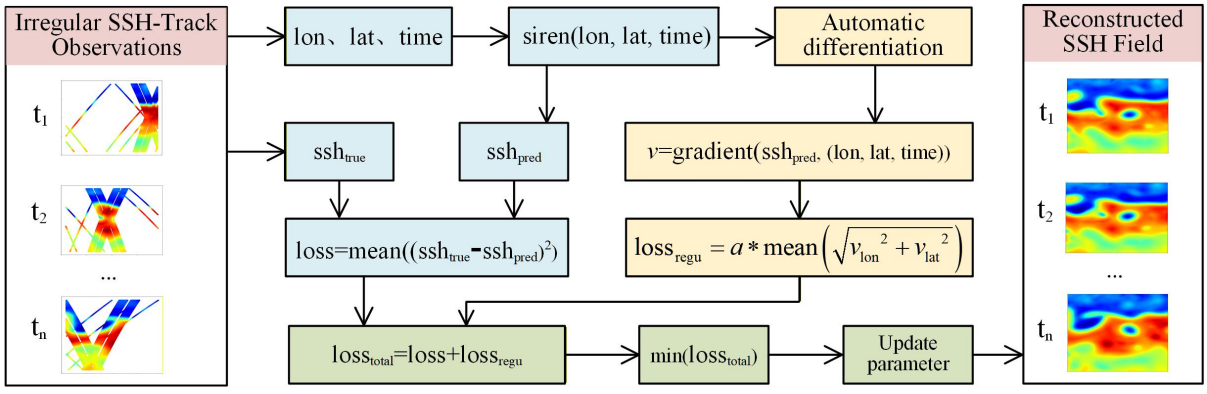

Figure 1. Architecture of the proposed INR-based SSH reconstruction framework, combining INR with TV regularization.

5 Experiment

Two experiments were designed to evaluate the performance and generalization capability of the proposed INR-based SSH reconstruction framework, with all experiments implemented using the publicly available code (Li, 2025b). All datasets used in this study originate from the Ocean Data Challenges initiative and have been archived at Zenodo to ensure accessibility and reproducibility (Li, 2025a). The first experiment uses real satellite altimetry observations collected in the Western Mediterranean Sea (MEDIT) within the domain $[1°\text{E} \times 20°\text{E}, 30°\text{N} \times 45°\text{N}]$, as illustrated in Figure 2. A subset of along-track SSH measurements is used for training, while the remaining observations serve as ground truth for validation. The second experiment is conducted using simulated SSH fields from the NATL60 nature run over a dynamically active portion of the Gulf Stream region (GF), spanning $[65°\text{W} \times 55°\text{W}, 33°\text{N} \times 43°\text{N}]$, as also shown in Figure 2. Pseudo-altimetric nadir and SWOT datasets are generated by realistically subsampling the NATL60 fields according to representative satellite constellations.

Using both observed and simulated SSH serves complementary purposes: experiments based on real altimetry provide a realistic assessment under actual sampling patterns and measurement uncertainties, whereas experiments based on NATL60 enable evaluation against a known reference field, thus allowing controlled examination of the ability of the method to recover fine-scale structures and quantify effective resolution. Taken together, these two experiments provide a comprehensive evalua-

https://doi.org/10.5194/egusphere-2025-6389
Preprint. Discussion started: 24 February 2026

tion of both practical applicability and intrinsic reconstruction capability of the proposed INR-based framework. Details of the evaluation metrics used in both experiments are summarized in Sect. 5.1.

Figure 2. Geographical domains used in the experiments: Western Mediterranean (MEDIT) and Gulf Stream (GF) regions.

5.1 Evaluation Indexes

To quantitatively assess reconstruction performance, three complementary metrics are used: pointwise error, normalized accuracy score, and spatio-temporal spectral fidelity.

(1) Root Mean Square Error (RMSE). The RMSE between reconstructed and true SSH is computed as:

$$\mathrm{RMSE} = \sqrt{\frac{1}{N}\sum_{i=1}^{N}\left[\mathrm{SSH}_{\mathrm{rec}}(\mathrm{lon}_i,\mathrm{lat}_i,\mathrm{time}_i) - \mathrm{SSH}_{\mathrm{true}}(\mathrm{lon}_i,\mathrm{lat}_i,\mathrm{time}_i)\right]^2}, \tag{10}$$

where N denotes the number of evaluation points. $\mathrm{SSH}_{\mathrm{rec}}(\mathrm{lon}_i,\mathrm{lat}_i,\mathrm{time}_i)$ is the reconstructed SSH at the i-th spatio-temporal location, and $\mathrm{SSH}_{\mathrm{true}}(\mathrm{lon}_i,\mathrm{lat}_i,\mathrm{time}_i)$ is the corresponding reference SSH value.

(2) RMSE-based score. A normalized accuracy score is defined as:

$$\mathrm{RMSE}_S = 1 - \frac{\mathrm{RMSE}}{\mathrm{RMS}(\mathrm{SSH}_{\mathrm{true}})}, \tag{11}$$

where $\mathrm{RMS}(\cdot)$ denotes the root-mean-square of the reference SSH field. A score of 1 corresponds to a perfect reconstruction.

(3) Wavenumber–frequency spectral score. To assess spectral consistency, we compute the wavenumber–frequency power spectral density score:

$$\mathrm{PSD}_S^{wf} = 1 - \frac{\mathrm{PSD}^{wf}(\mathrm{SSH}_{\mathrm{rec}} - \mathrm{SSH}_{\mathrm{true}})}{\mathrm{PSD}^{wf}(\mathrm{SSH}_{\mathrm{true}})}, \tag{12}$$

https://doi.org/10.5194/egusphere-2025-6389
Preprint. Discussion started: 24 February 2026

where $\mathrm{PSD}^{wf}(\cdot)$ denotes the wavenumber–frequency power spectral density.

Two characteristic spectral resolutions are also derived from the wavenumber–frequency power spectral density, denoted as λ_x and λ_t. The quantity λ_x (in degrees) represents the minimum resolvable spatial wavelength, while λ_t (in days) denotes the minimum resolvable temporal wavelength. Both metrics are defined using the standard 0.5-contour level of the normalized spectral score PSD_S^{wf}, providing a consistent measure of the smallest scales that the reconstruction method can reliably resolve.

5.2 Implementation details

The proposed INR-based reconstruction framework is implemented in PyTorch. Unless otherwise specified, the SIREN model is configured with three hidden layers , each containing 256 units. Following established INR design principles, the first layer is initialized with an elevated angular frequency (first_$\omega_0 = 10$) to enhance the representation of fine-scale spatial structures, while the hidden layers employ a larger frequency factor (hidden_$\omega_0 = 30$) to increase the network's spectral expressiveness. Model parameters are optimized using the Adam optimizer with an initial learning rate of 1×10^{-4}. All experiments are conducted on a single NVIDIA GPU within a controlled computational environment to ensure reproducibility.

5.3 Observed SSH Experiment

This experiment aims to evaluate the capability of the proposed method to reconstruct sequences of SSH maps from incomplete real-world satellite altimetry measurements. All observations used in this section originate from operational nadir altimeters and correspond to actual SSH acquisitions.

5.3.1 Data Preparation

The study focuses on the Western Mediterranean Sea, defined by the region $[1°\mathrm{E} \times 20°\mathrm{E}, 30°\mathrm{N} \times 45°\mathrm{N}]$. The SSH data used in this analysis includes altimeter measurements from several satellites: SARAL/Altika (alg), Haiyang-2B (h2b), Jason 3 (j3), Sentinel 3A (s3a), Sentinel 3B (s3b), and the new orbit of Cryosat-2 (c2n). This constellation of nadir altimeters was operational and will be investigated during the period from January 1, 2021, to March 31, 2021, and will be analyzed in this study. Specifically, the SSH data from SARAL/Altika, Haiyang-2B, Jason 3, Sentinel 3A, and Sentinel 3B are used as training data, while the data from Cryosat-2's new orbit are reserved for testing. The training data spans from January 1, 2021, to January 15, 2021, and from March 15, 2021, to March 31, 2021, while the test data covers the period from January 15, 2021, to March 15, 2021.

5.3.2 Experiment design

Two classes of comparative experiments are conducted to assess reconstruction performance.

(1) Comparison with optimal interpolation (OI). We first compare our approach with the optimal interpolation (OI), which serves as the present-day standard for DUACS products provided by AVISO. This detailed comparison is conducted from

https://doi.org/10.5194/egusphere-2025-6389
Preprint. Discussion started: 24 February 2026

multiple perspectives, including the orbital distribution of absolute errors, the spatial distribution of residuals on the grid, the temporal evolution of the RMSE-based score, and the spectral performance assessed via PSD.

(2) Comparison with state-of-the-art methods. Second, to further validate the robustness and general applicability of our approach, we compare it with several representative state-of-the-art methods, namely the Covariance-based optimal interpolation (BASELINE OI), the back-and-forth nudging algorithm combined with a quasigeostrophic model (BFN_QG) (Le Guillou et al., 2023), BFN_QG with Dirichlet boundary conditions (BFN_QG with coasts), and Wavevar (Ubelmann et al., 2021).

5.3.3 Detailed Comparison with Optimal Interpolation

(1) Along-track Absolute SSH Errors. Figure 3 shows the absolute SSH error along the CryoSat-2 new orbit. Along the satellite tracks, INR systematically yields smaller errors than OI. The error distribution produced by INR is also more spatially uniform, exhibiting fewer isolated spikes or abrupt deviations. This improvement arises from the continuity of the SIREN representation and the ability to compute analytical derivatives, which allows the TV regularization to impose precise gradient constraints and preserve sharp transitions. Consequently, INR stabilizes interpolation along individual altimetric tracks and better captures local-scale SSH variations, even in regions with sparse sampling or energetic dynamics.

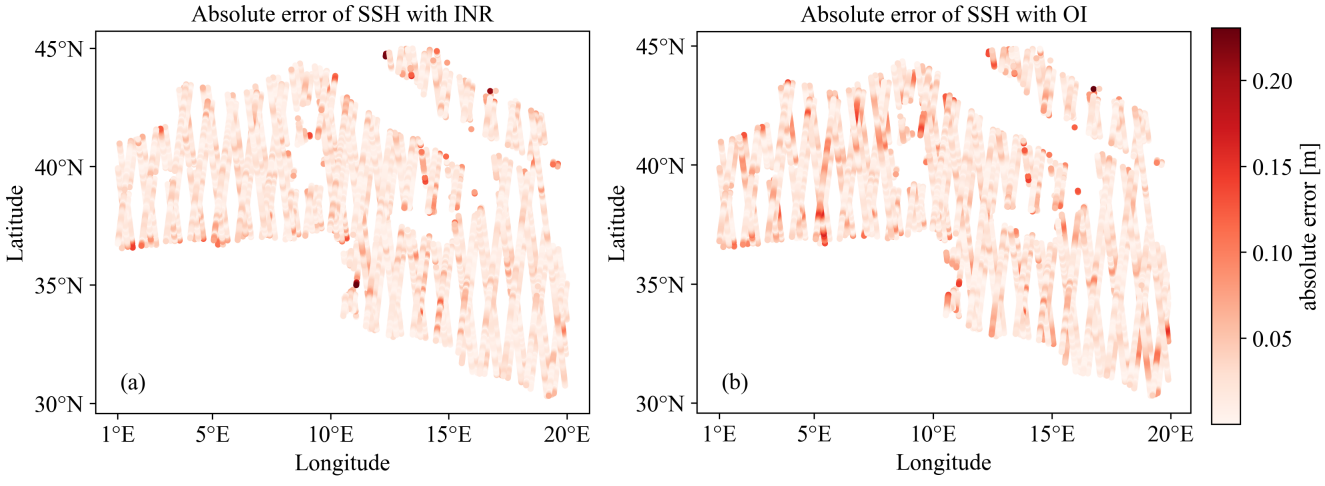

Figure 3. Absolute SSH reconstruction errors computed along the CryoSat-2 orbit (a) Errors produced by the proposed INR-based framework, and (b) errors obtained from the conventional OI method.

(2) Gridded Spatial RMSE. The gridded RMSE computed from Eq. (10) for the different reconstruction methods is shown in Figure 4. Overall, the INR–based reconstruction exhibits smaller RMSE values than the OI scheme over most of the domain, indicating a systematically improved fit to the reference SSH field. Regions with comparatively large errors are present for both methods and are mainly located near the boundaries of the reconstruction domain, where the observational coverage is sparse and the extrapolation component of the mapping problem becomes more pronounced.

https://doi.org/10.5194/egusphere-2025-6389
Preprint. Discussion started: 24 February 2026

In these boundary areas, however, the INR method yields noticeably fewer grid points with high RMSE than OI. This improvement can be related to the properties of the proposed framework: the INR provides a globally continuous mapping from spatio-temporal coordinates to SSH, which avoids grid-induced discontinuities, while the TV regularization constrains spurious oscillations and suppresses noise-driven gradients. As a result, the reconstructed field remains coherent in poorly sampled edge regions without excessively smoothing sharp transitions, leading to a more accurate and spatially consistent RMSE pattern compared with the classical OI approach.

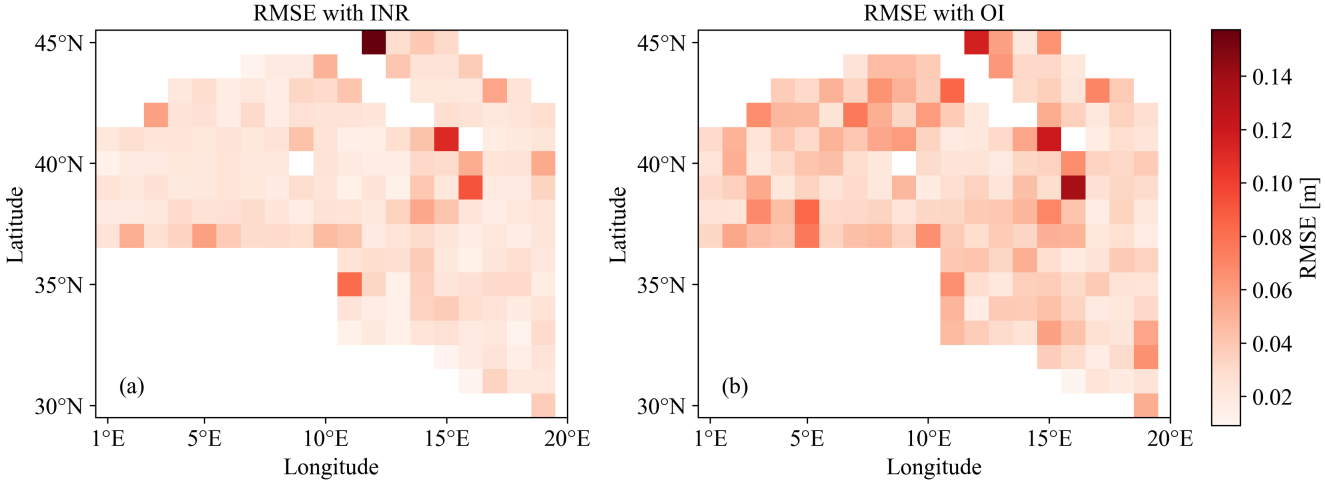

Figure 4. Spatial distribution of RMSE for the mapped SSH fields obtained with (a) the INR-based framework and (b) the conventional OI method.

(3) Temporal Performance: RMSE-based Score. The temporal behaviour of the reconstruction is assessed using the RMSE-based score ($RMSE_S$), computed according to Eq. (11) and shown in Figure 5. Figure 5(b) indicates several distinct drops (e.g. around 22 January, 8 February, and 20 February), which correspond to pronounced temporal variations in the observed SSH shown in Figure 5(a). These episodes highlight periods of increased reconstruction difficulty. Despite these abrupt transitions, INR consistently yields higher $RMSE_S$ values than OI throughout the examined period. This advantage can be linked to the continuous implicit representation learned by INR, which provides a smoother yet flexible temporal interpolation, and to the TV regularization, which suppresses spurious oscillations while preserving physically meaningful sharp variations. As a consequence, INR remains closer to the observed SSH during periods of strong temporal gradients, resulting in systematically improved temporal performance compared with the classical OI approach.

https://doi.org/10.5194/egusphere-2025-6389
Preprint. Discussion started: 24 February 2026

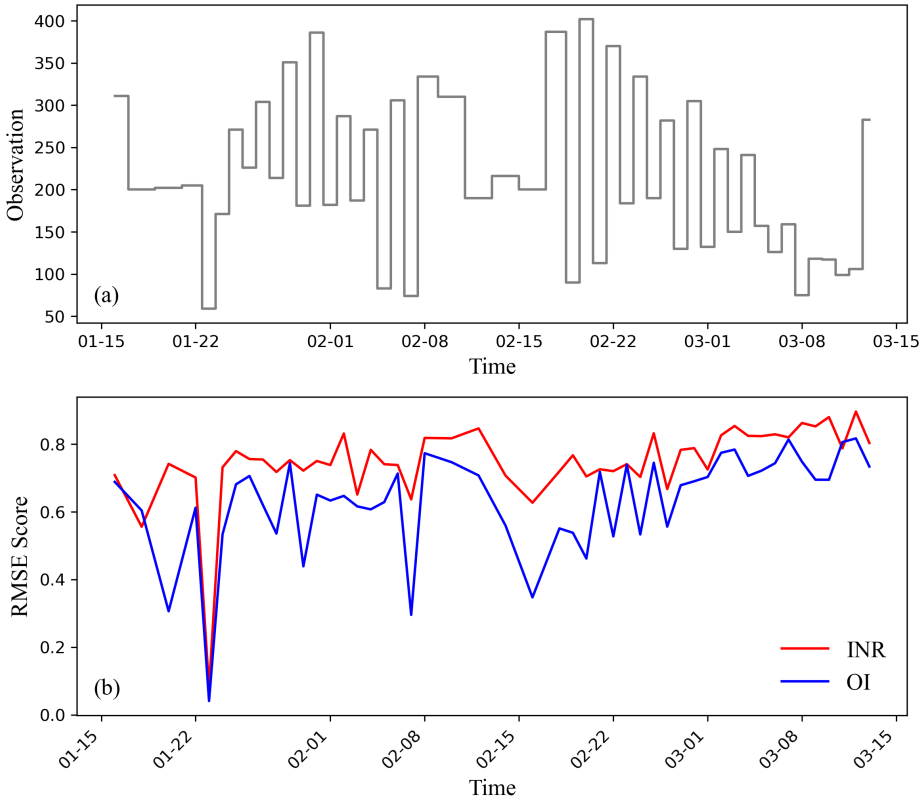

Figure 5. Temporal evolution of the RMSE-based score defined in Eq. (11). (a) Along-track SSH time series extracted at the CryoSat-2 observation points, showing several periods of strong temporal variability. (b) Corresponding RMSE-based score RMSE_S for the INR and OI reconstructions.

(4) Spectral Diagnostics and Effective Resolution Spectral diagnostics are presented in Figure 6. Figure 6(a) shows the wavenumber–frequency power spectral density (PSD^{wf}). The SSH field reconstructed via INR more closely matches the true PSD^{wf} derived from observations, indicating improved preservation of the energy distribution across spatial and temporal scales. Figure 6(b) shows the corresponding spectral score, where intersections with the 0.5 contour indicate effective resolutions. Across all scales, INR achieves higher spectral scores than OI. Notably, INR resolves spatial scales down to 106 km, whereas OI resolves only to 154 km. This gain can be attributed to the sinusoidal representation in SIREN, which alleviates spectral bias and enables the network to represent higher-frequency components associated with small-scale SSH variability. In addition, the TV regularisation mitigates unwanted oscillations during reconstruction and helps preserve sharp gradients, thereby improving the fidelity of fine-scale structures.

https://doi.org/10.5194/egusphere-2025-6389
Preprint. Discussion started: 24 February 2026

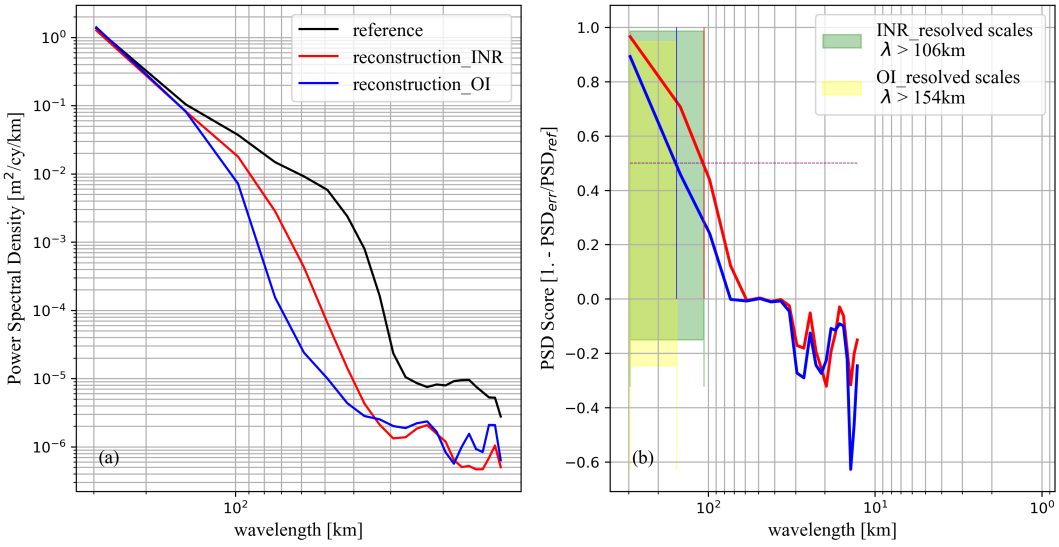

Figure 6. Spectral diagnostics of the reconstructed SSH fields. (a) Wavenumber–frequency power spectral density (PSD^{wf}) of the INR reconstruction compared with the reference and OI. (b) Corresponding PSD^{wf} score, where the intersection with the 0.5 contour indicates the effective spatial resolution. Higher scores across a wider range of wavenumbers illustrate the improved capability of the proposed INR framework in recovering fine-scale SSH variability.

5.3.4 Comprehensive Comparison with Multiple Methods

This section provides a broader evaluation of the proposed approach by comparing it against several representative reconstruction methods. The assessment relies on the two quantitative metrics introduced in Sect. 5.1, namely the mean RMSE-based score $u(\mathrm{RMSE}_S)$ and the shortest resolved spatial scale λ_x. The results are summarized in Table 1. A key point is that global accuracy metrics such as $u(\mathrm{RMSE}_S)$ are strongly influenced by large-scale SSH variability, which dominates the total variance of the field. Methods that capture these large-scale components well may obtain high $u(\mathrm{RMSE}_S)$ values even if their reconstruction of finer-scale structures remains limited. In contrast, although small-scale features contribute relatively little to global error statistics, they are dynamically important and determine the effective spatial resolution.

In this context, while INR attains a slightly lower $u(\mathrm{RMSE}_S)$ than the best-performing method, it achieves the smallest λ_x, indicating the highest spatial resolution among all approaches. This balance results from the design of INR: the SIREN representation provides a continuous and coherent functional mapping over the entire domain, whereas the TV regularization constrains gradients and preserves sharp transitions. As a result, INR captures fine-scale SSH variability without substantially compromising large-scale accuracy, yielding a reconstruction that is both globally consistent and highly resolved.

https://doi.org/10.5194/egusphere-2025-6389
Preprint. Discussion started: 24 February 2026

Table 1. Results of different methods using satellite altimetry observations in the Mediterranean region. Bold values denote best performance.

Method	$u(\mathrm{RMSE}_S)$	λ_x (km)
OI	0.674136	148
BFN_QG	0.720857	125
BFNQG_coast	0.724554	125
WaveVar	**0.759956**	118
INR	0.747545	**106**

5.4 Simulated SSH Experiment

This section evaluates the proposed method using simulated SSH data. Unlike real altimetric observations, the model generates complete reference SSH fields, enabling detailed quantitative assessment of interpolation accuracy and effective spatio-temporal resolution.

5.4.1 Data Preparation

To assess the accuracy of the reconstructed SSH, satellite altimetry data are generated using model simulation data for model training, while model data corresponding to missing values are employed as validation data for model verification. Specifically, NATL60 simulations, based on the Nucleus for European Modelling of the Ocean (NEMO) (Ajayi et al., 2020) and conducted without tidal forcing, are utilized to simulate the sea surface height in the Gulf Stream region for the period from October 1, 2012, to September 30, 2013. Subsequently, the corresponding satellite altimetry data are simulated using the orbital coordinates and repeat cycles of various satellites, including Topex-Poseidon, Jason 1, Geosat Follow-On, Envisat, and SWOT altimeters. Specifically, data from January 2, 2013, to September 30, 2013, are used for training, while data from October 22, 2012, to December 2, 2012, serve as the test data.

5.4.2 Experiment design

The experimental setup aims to comprehensively evaluate the proposed approach's performance and robustness. First, we focus on comparing the reconstructed SSH with the model-simulated SSH, evaluating the accuracy from both direct SSH comparisons and the calculation of higher-order derivatives to assess how well the method captures the underlying spatial dynamics. Second, to further validate the general applicability of our method, we compare it with several existing state-of-the-art interpolation and reconstruction methods, including DUACS (traditional covariance-based optimal interpolatio(Taburet et al., 2019)),three model-based data assimilation schemes: BFN(a data assimilation method that follows quasi-geostrophic dynamics(Le Guillou et al., 2021)), DYMOST (dynamic OI accounting for the SSH nonlinear temporal propagation(Ubelmann et al., 2016)), MIOST (multiscale OI (Ardhuin et al., 2022)). Finally, we compare with the supervised 4DVarNet(based on a neural network architecture backed by a variational formulation(Beauchamp et al., 2023)). Performance is assessed using the

https://doi.org/10.5194/egusphere-2025-6389
Preprint. Discussion started: 24 February 2026

statistical metrics defined in Sect. 5.1, including the mean RMSE-based score $u(\mathrm{RMSE}_S)$ and the spectral metrics λ_x and λ_t, which together characterize both reconstruction accuracy and the smallest spatial and temporal scales that each method can resolve.

5.4.3 Evaluation of Reconstructed Sea Surface Height

Figure 7 illustrates the INR–based SSH reconstruction at four randomly selected times ($\mathrm{t}_1, \mathrm{t}_2, \mathrm{t}_3, \mathrm{t}_4$). The first row shows the along-track observations used for reconstruction, where the slightly thicker tracks correspond to simulated SWOT measurements. As expected in realistic multi-mission sampling, the spatial coverage and density of satellite swaths vary significantly among time steps, introducing substantial challenges for reconstructing a spatially continuous SSH field.

The second row displays the fully reconstructed SSH maps produced by the proposed INR-based framework. The spatial structure of mesoscale eddies is consistently recovered across all four snapshots, including their positions, amplitudes, and morphological asymmetries. This capability is primarily enabled by the SIREN-based implicit representation, which provides sufficient spectral flexibility to represent higher-frequency components beyond the limitations of grid-based interpolation. In parallel, the TV regularization imposes a constraint on spatial gradients of the reconstructed SSH field, limiting over-smoothing and preventing the emergence of artificial oscillations. The combined effect of these two components yields reconstructions that preserve both large-scale coherence and sharp local transitions, even under sparse and irregular sampling conditions.

A key advantage of the INR framework is that it produces a continuous and differentiable functional representation of SSH. Leveraging this property, the third row presents the corresponding first-order spatial gradients, which reveal fine-scale structures such as eddy peripheries and frontal regions that are critical for interpreting dynamical processes. These gradient fields are computed analytically through SIREN's sinusoidal activations, avoiding numerical differentiation and maintaining high precision.

While Figure 7 provides a snapshot-based assessment, the full temporal evolution of the along-track observations, the reconstructed SSH fields, and the corresponding SSH gradient norms is presented in Supplementary Video S1. This video further illustrates the temporal continuity of the implicit representation and the stability of fine-scale structures over time. Collectively, the results demonstrate that INR provides high-fidelity SSH reconstructions even in the presence of irregular and temporally varying sampling patterns, while its differentiable representation enables higher-order analysis of oceanic features.

https://doi.org/10.5194/egusphere-2025-6389
Preprint. Discussion started: 24 February 2026

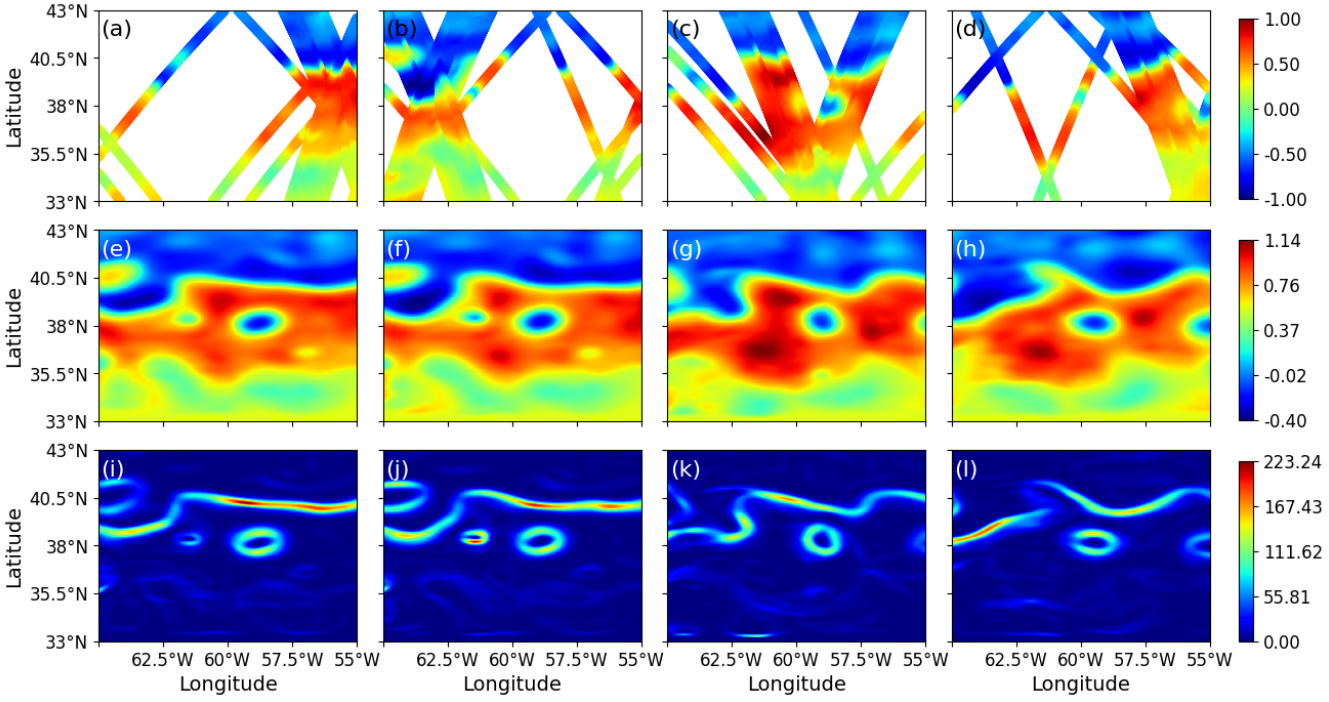

Figure 7. Along-track SSH observations (top row), reconstructed SSH fields (middle row), and the norm of the SSH gradient (bottom row) shown at four representative time steps. An animated version illustrating the full temporal evolution is provided as Supplementary Video S1 (https://doi.org/10.5281/zenodo.17991117).

5.4.4 Comparison of Multiple Methods for SSH Reconstruction

Table 2 reports the performance of the proposed INR method in comparison with several representative state-of-the-art approaches. In terms of the normalized RMSE score $u(\text{RMSE})$, INR performs on par with the top-performing schemes. Although its $u(\text{RMSE})$ value is slightly lower than that of 4DVarNet v2022, INR achieves the highest effective spatial and temporal resolutions among all evaluated methods. In particular, INR attains the smallest resolved spatial wavelength λ_x and temporal wavelength λ_t. These gains can be interpreted in light of the INR formulation: the sinusoidal building blocks of SIREN reduce spectral bias and allow the representation of higher-frequency components, while the continuous and differentiable nature of the implicit model permits analytical gradients that preserve sharp SSH variations. Together with the TV regularisation that discourages spurious oscillations, this yields reconstructions that retain finer-scale structures than methods relying on predefined covariance models or dynamical constraints.

Overall, INR maintains competitive global accuracy while substantially enhancing the reconstruction of mesoscale and submesoscale patterns. This balance indicates that the proposed approach provides SSH fields with improved spatial–temporal resolution, complementing classical interpolation and data-assimilation techniques.

https://doi.org/10.5194/egusphere-2025-6389
Preprint. Discussion started: 24 February 2026

Table 2. Results of different methods using the simulated altimetry dataset in the Gulf Stream domain. Bold values denote best performance.

Method	u(RMSE)	λ_x (degree)	λ_t (days)
DUACS	0.92	1.22	11.37
BFN	0.93	1.00	10.24
DYMOST	0.93	1.19	10.04
MIOST	0.94	1.18	10.33
4DVarNet	0.95	0.70	6.48
4DVarNet v2022	**0.96**	0.62	4.35
INR	0.94	**0.03**	**2.05**

6 Conclusion and Discussion

This study proposed an INR framework for SSH reconstruction, combining the SIREN with TV regularization. The SIREN component provides a continuous and highly expressive functional mapping with analytically computable derivatives, while the TV term constrains spatial gradients to preserve fronts, eddy peripheries, and other sharp structures. Together, these components yield a compact and differentiable representation capable of reconstructing both smooth large-scale variability and fine-scale features. Comprehensive experiments using real altimetric observations and high-resolution simulated SSH demonstrate that the proposed framework outperforms conventional optimal interpolation schemes and several state-of-the-art reconstruction approaches. The method exhibits competitive or superior global accuracy while achieving substantially finer effective spatial and temporal resolution. Notably, the differentiable nature of the INR allows for direct computation of spatial derivatives, enabling more reliable characterization of mesoscale and submesoscale dynamics compared with grid-based methods that rely on numerical differencing.

These findings suggest that INR-based framework offer a promising alternative to traditional SSH interpolation and data-assimilation techniques, particularly in contexts involving sparse, irregular, or multi-mission satellite sampling. Future work should explore the incorporation of additional observational modalities, such as sea surface temperature or ocean color, in order to improve the spatial and temporal coverage and enhance physical consistency. Another perspective is to integrate explicit dynamical constraints or physical priors, with the aim of further improving interpretability and operational applicability. The combination of implicit representations with oceanographic knowledge offers a useful direction for advancing high-resolution and dynamically coherent reconstruction of ocean surface variability.

Code availability. The source code used in this study is publicly available at https://doi.org/10.5281/zenodo.18019725(Li, 2025b). The repository includes all scripts necessary to reproduce the main experiments.

https://doi.org/10.5194/egusphere-2025-6389
Preprint. Discussion started: 24 February 2026

Data availability. The datasets analysed in this study are provided by the Ocean Data Challenges initiative maintained by AVISO and are archived at Zenodo: https://doi.org/10.5281/zenodo.18748410 (Li, 2025a).

Author contributions. Dongshuang Li led the development of the methodology, implemented the model, performed the numerical experiments, carried out the data analysis, and drafted the manuscript. Liming Pan supervised the research, contributed to the conceptual design and technical refinement of the methodology, and provided substantial revisions to the manuscript. Zhaoyuan Yu contributed to data preparation, experimental design discussions, and interpretation of the results. Linwang Yuan contributed to the development of the workflow, assisted with visualization and validation of the model outputs. All authors reviewed and approved the final manuscript.

Competing interests. The authors declare that they have no conflict of interest.

Acknowledgements. This research was supported by the National Natural Science Foundation of China (Grant Nos. 42476191, 42130103 and 42230406). The authors acknowledge the Ocean Data Challenges community for providing open access to the datasets used in this study. We also thank our colleagues for their constructive comments and discussions during the development of this work.

https://doi.org/10.5194/egusphere-2025-6389
Preprint. Discussion started: 24 February 2026

References

Ajayi, A., Le Sommer, J., Chassignet, E., Molines, J.-M., Xu, X., Albert, A., and Cosme, E.: Spatial and temporal variability of the North Atlantic eddy field from two kilometric-resolution ocean models, Journal of Geophysical Research: Oceans, 125, e2019JC015 827, 2020.

Ardhuin, F., Ubelmann, C., Dibarboure, G., Gaultier, L., Ponte, A., Ballarotta, M., and Faugère, Y.: Reconstructing ocean surface current combining altimetry and future spaceborne doppler data, Authorea Preprints, 2022.

Beauchamp, M., Febvre, Q., Georgenthum, H., and Fablet, R.: 4DVarNet-SSH: End-to-end learning of variational interpolation schemes for nadir and wide-swath satellite altimetry, Geoscientific Model Development, 16, 2119–2147, 2023.

Camargo, C. M., Riva, R. E., Hermans, T. H., Schütt, E. M., Marcos, M., Hernandez-Carrasco, I., and Slangen, A. B.: Regionalizing the sea-level budget with machine learning techniques, Ocean Science, 19, 17–41, 2023.

Denvil-Sommer, A., Buitenhuis, E. T., Kiko, R., Lombard, F., Guidi, L., and Le Quéré, C.: Testing the reconstruction of modelled particulate organic carbon from surface ecosystem components using PlankTOM12 and machine learning, Geoscientific Model Development, 16, 2995–3012, 2023.

Fablet, R., Beauchamp, M., Drumetz, L., and Rousseau, F.: Joint interpolation and representation learning for irregularly sampled satellite-derived geophysical fields, Frontiers in Applied Mathematics and Statistics, 7, 655 224, 2021.

Genova, K., Cole, F., Vlasic, D., Sarna, A., Freeman, W. T., and Funkhouser, T.: Learning shape templates with structured implicit functions, in: Proceedings of the IEEE/CVF International Conference on Computer Vision, pp. 7154–7164, 2019.

Guan, Y., Chubarau, A., Rao, R., and Nowrouzezahrai, D.: Learning neural implicit representations with surface signal parameterizations, Computers & Graphics, 114, 257–264, 2023.

Huang, Z., Bai, S., and Kolter, J. Z.: Implicit Layers for Implicit Representations, Advances in Neural Information Processing Systems, 34, 9639–9650, 2021.

Le Guillou, F., Metref, S., Cosme, E., Ubelmann, C., Ballarotta, M., Le Sommer, J., and Verron, J.: Mapping altimetry in the forthcoming swot era by back-and-forth nudging a one-layer quasigeostrophic model, Journal of Atmospheric and Oceanic Technology, 38, 697–710, 2021.

Le Guillou, F., Gaultier, L., Ballarotta, M., Metref, S., Ubelmann, C., Cosme, E., and Rio, M.-H.: Regional mapping of energetic short mesoscale ocean dynamics from altimetry: performances from real observations, Ocean Science, 19, 1517–1527, 2023.

Le Traon, P. and Dibarboure, G.: Mesoscale mapping capabilities of multiple-satellite altimeter missions, Journal of Atmospheric and Oceanic Technology, 16, 1208–1223, 1999.

Li, D.: Dataset for "A Continuous Implicit Neural Representation Framework with Gradient Regularization for Sea Surface Height Reconstruction From Satellite Altimetry", https://doi.org/10.5281/zenodo.18748410, 2025a.

Li, D.: Code for: Continuous Implicit Neural Representation Framework with Gradient Regularization for Sea Surface Height Reconstruction from Satellite Altimetry, https://doi.org/10.5281/zenodo.18019725, 2025b.

Lou, R., Lv, Z., Dang, S., Su, T., and Li, X.: Application of machine learning in ocean data, Multimedia Systems, 29, 1815–1824, 2023.

Manucharyan, G. E., Siegelman, L., and Klein, P.: A deep learning approach to spatiotemporal sea surface height interpolation and estimation of deep currents in geostrophic ocean turbulence, Journal of Advances in Modeling Earth Systems, 13, e2019MS001 965, 2021.

Molaei, A., Aminimehr, A., Tavakoli, A., Kazerouni, A., Azad, B., Azad, R., and Merhof, D.: Implicit neural representation in medical imaging: A comparative survey, in: Proceedings of the IEEE/CVF International Conference on Computer Vision, pp. 2381–2391, 2023.

https://doi.org/10.5194/egusphere-2025-6389
Preprint. Discussion started: 24 February 2026

Oechsle, M., Mescheder, L., Niemeyer, M., Strauss, T., and Geiger, A.: Texture fields: Learning texture representations in function space, in: Proceedings of the IEEE/CVF International Conference on Computer Vision, pp. 4531–4540, 2019.

Shi, J. and Jin, T.: Suitable region of dynamic optimal interpolation for efficiently altimetry sea surface height mapping, Geodesy and Geodynamics, 15, 142–149, 2024.

Sitzmann, V., Zollhöfer, M., and Wetzstein, G.: Scene representation networks: Continuous 3d-structure-aware neural scene representations, Advances in Neural Information Processing Systems, 32, 2019.

Sitzmann, V., Martel, J., Bergman, A., Lindell, D., and Wetzstein, G.: Implicit neural representations with periodic activation functions, Advances in neural information processing systems, 33, 7462–7473, 2020.

Srinivasan, M. and Tsontos, V.: Satellite Altimetry for Ocean and Coastal Applications: A Review, Remote Sensing, 15, 3939, 2023.

Stegner, A., Le Vu, B., Dumas, F., Ghannami, M. A., Nicolle, A., Durand, C., and Faugere, Y.: Cyclone-anticyclone asymmetry of eddy detection on gridded altimetry product in the Mediterranean Sea, Journal of Geophysical Research: Oceans, 126, e2021JC017 475, 2021.

Taburet, G., Sanchez-Roman, A., Ballarotta, M., Pujol, M.-I., Legeais, J.-F., Fournier, F., Faugere, Y., and Dibarboure, G.: DUACS DT2018: 25 years of reprocessed sea level altimetry products, Ocean Science, 15, 1207–1224, 2019.

Tancik, M., Srinivasan, P., Mildenhall, B., Fridovich-Keil, S., Raghavan, N., Singhal, U., Ramamoorthi, R., Barron, J., and Ng, R.: Fourier features let networks learn high frequency functions in low dimensional domains, Advances in neural information processing systems, 33, 7537–7547, 2020.

Ubelmann, C., Klein, P., and Fu, L.-L.: Dynamic interpolation of sea surface height and potential applications for future high-resolution altimetry mapping, Journal of Atmospheric and Oceanic Technology, 32, 177–184, 2015.

Ubelmann, C., Cornuelle, B., and Fu, L.-L.: Dynamic mapping of along-track ocean altimetry: Method and performance from observing system simulation experiments, Journal of Atmospheric and Oceanic Technology, 33, 1691–1699, 2016.

Ubelmann, C., Dibarboure, G., Gaultier, L., Ponte, A., Ardhuin, F., Ballarotta, M., and Faugère, Y.: Reconstructing ocean surface current combining altimetry and future spaceborne Doppler data, Journal of Geophysical Research: Oceans, 126, e2020JC016 560, 2021.

Wiesner, D., Suk, J., Dummer, S., Svoboda, D., and Wolterink, J. M.: Implicit neural representations for generative modeling of living cell shapes, in: International Conference on Medical Image Computing and Computer-Assisted Intervention, pp. 58–67, Springer, 2022.

Xu, D., Wang, P., Jiang, Y., Fan, Z., and Wang, Z.: Signal processing for implicit neural representations, Advances in Neural Information Processing Systems, 35, 13 404–13 418, 2022.

Ye, J., Chen, Y., Wang, N., and Wang, X.: Gifs: Neural implicit function for general shape representation, in: Proceedings of the IEEE/CVF Conference on Computer Vision and Pattern Recognition, pp. 12 829–12 839, 2022.